[CANCER RESEARCH 61, 538–549, January 15, 2001]

Deregulated Expression of c-*mos* in Non-Small Cell Lung Carcinomas: Relationship with *p53* Status, Genomic Instability, and Tumor Kinetics

Vassilis G. Gorgoulis,[1] Panayotis Zacharatos, George Mariatos, Triantafillos Liloglou, Stavros Kokotas, Nikolaos Kastrinakis, Athanassios Kotsinas, Athanassios Athanasiou, Pericles Foukas, Vassilios Zoumpourlis, Dimitris Kletsas, John Ikonomopoulos, Panayiotis J. Asimacopoulos, Christos Kittas, and John K. Field

Departments of Histology and Embryology, School of Medicine [V. G. G., P. Z., G. M., S. K., N. K., A. K., A. A., P. F., J. I., C. K.], and Cardiac Surgery [P. J. A.], University of Athens, Athens, Greece; Roy Castle International Centre for Lung Cancer Research, Liverpool, United Kingdom [V. G. G., P. Z., T. L., J. K. F.]; Bristol Heart Institute, University of Bristol, Bristol, United Kingdom [A. A.]; Institute of Biological Research and Biotechnology, National Hellenic Research Foundation, Athens, Greece [V. Z.]; Laboratory of Cell Proliferation and Ageing, Institute of Biology, NCSR "Demokritus," Athens, Greece [D. K.]; and Baylor College of Medicine, Houston, Texas 77030 [P. J. A.]

ABSTRACT

Little is known about the status of the mitogen-activating protein kinase pathways in lung cancer. One of the key molecules taking part in these pathways is the product of the c-*mos* proto-oncogene, which plays an important role in oocyte maturation. *In vitro* investigations in somatic cells have shown that c-*mos* expression has opposing effects on the cell cycle, which suggests that this proto-oncogene may represent an important determinant of aberrant cell function (genomic instability and altered kinetics). A recent study suggests that these effects may be p53 dependent. In view of the apparent link between c-mos and p53, we investigated in a series of 56 non-small cell lung carcinomas: *a*) the status of c-*mos*; *b*) its relationship to genomic instability (aneuploidy) and two kinetic parameters of the tumors, proliferation and apoptotic indexes (AI); and *c*) its association with *p53* alterations and their concomitant relationship with the above parameters.

We found c-mos overexpression in 27% of the tumors. Expression was higher in stages II/III (34%) than in stage I (17%; $P = 0.018$). Complete concordance was observed between c-mos overexpression and elevated c-*mos* mRNA levels. Because c-*mos* gene amplification was not detected, its deregulated expression may be attributable to increased transcription. Of the c-mos positive [c-mos(P)] cases, 77% were associated with aneuploidy. Sequencing showed two silent mutations and one missense (R→L) at codon 22, located in a region critical for c-mos stability. In contrast to the findings of some *in vitro* studies, c-mos(P) tumors had a lower mean AI score than the c-mos negative [c-mos(N)] tumors had, implying that induction of apoptosis may have been defective. Indeed, 86% of the tumors overexpressing c-mos showed *p53* alterations. The carcinomas with concomitant alterations of c-mos and p53 [c-mos(P)/p53 positive] had significantly lower AI values ($P < 0.001$) and were more frequently associated with aneuploidy ($P = 0.015$) than the c-mos(N)/p53 negative tumors but not the c-mos(N)/p53 positive tumors, which suggests that p53 status is the main determinant of ploidy status and apoptosis in our series. This finding also strengthens the concept that wild-type p53 plays a "safeguard" role in preventing oncogene-mediated activation.

INTRODUCTION

Genomic instability is a hallmark of malignant cells and occurs either in the form of microsatellite instability or in the form of CIN (1).[2] Microsatellite instability is reflected by alterations in polymorphic, short, tandem repeat sequences and is associated in a small fraction of colorectal carcinomas with germ-line or somatic mutations of the DNA mismatch repair genes (2). On the other hand, CIN, which represents gains or losses of segments or whole chromosomes and leads to abnormal numbers of chromosomes (aneuploidy), is likely to occur in most human malignancies (1). The molecular basis of the latter is just beginning to be investigated. It is reasonable to suggest that alterations of the genes involved in replication, chromosome condensation, and segregation, as well as inactivation of checkpoint genes that monitor DNA damage and proper assembly of the spindle, represent the main events leading to CIN (3).

Of the rapidly increasing list of molecules that participate in the cell-cycle checkpoint pathways, p53 is the most widely studied. p53 is a transcription factor that mediates G_1 arrest in response to genotoxic stress, allowing time for DNA repair or apoptosis in case that repair is not feasible (4). It is also activated by oncogenic stimuli that trigger an antitumorigenic response (5) and by antimicrotubule drugs that elicit a G_2 arrest (6). Thus, p53 "senses" alterations at both checkpoints, G_1-S and G_2-M. These diverse "safeguard" properties of p53 make it the most common genetic target in human malignancies (7). Although the downstream effects of p53 have been investigated in detail (4), our knowledge about the upstream biochemical signals that activate p53 are still poorly understood. Increasing evidence suggests that phosphorylation is one type of upstream signal that triggers the p53 regulatory functions. p53 phosphorylation is mediated by several cellular kinases including ataxia-telangiectasia mutated kinase (8), DNA-dependent protein kinase (9), Jun-NH_2 kinase (10), casein kinases I and II, cyclin-activating kinase complex, and others (9). In a recent report, Fukasawa and Vande Woude (11) demonstrated *in vitro* that the levels of wt p53 increased in response to high mos/MAPK expression, which induces growth arrest or apoptosis depending on the phase of the cell cycle. They also observed that abrogation of *p53* was followed by a reduction of growth arrest, a 2–3-fold higher transformation efficiency of mos in mouse embryo fibroblasts, and chromosome instability.

The c-*mos* proto-oncogene is the cellular homologue of the *v-mos* oncogene, a product of Moloney murine sarcoma virus, identified in the early 1980s. It is located at chromosome region 8q11–12 and encodes a M_r 39,000 protein with serine-threonine kinase activity (12, 13). c-mos is an upstream activator of the MAPK pathway, phosphorylating MAPK kinase (14). It plays an important role in oocyte maturation, in which, as a component of the cytostatic factor, it arrests oocytes at metaphase II by stabilizing the maturation-promoting factor (14). Moreover, c-mos activity is associated with the appropriate formation and orientation of the meiotic spindle that leads to asymmetric division of the oocyte and the production of the first polar body (15). Although the role of c-*mos* in oocyte maturation is well established, very little is known about its expression and functions in human somatic cells (16). Constitutive expression of c-mos in somatic

Received 11/30/99; accepted 11/13/00.

The costs of publication of this article were defrayed in part by the payment of page charges. This article must therefore be hereby marked *advertisement* in accordance with 18 U.S.C. Section 1734 solely to indicate this fact.

[1] To whom requests for reprints should be addressed, at Antaiou 53 Str., Lamprini, Ano Patisia, Athens GR-11146, Greece. Phone: 30-1-6535894; Fax: 30-1-2928349; E-mail: histoclub@ath.forthnet.gr.

[2] The abbreviations used are: CIN, chromosomal instability; wt, wild-type; MAPK, mitogen-activated protein kinase; NSCLC, non-small cell lung carcinomas; PI, proliferation index; AI, apoptotic index; ERK, extracellular signal-regulated kinase; c-mos(P), c-mos positive; c-mos(N), c-mos negative; p53(P), p53 positive; p53(N), p53 negative; RT-PCR, reverse transcription PCR; D-PCR, differential PCR; SSCP, single strand conformation polymorphism; AIm, allelic imbalance; LOH, loss of heterozygosity; TUNEL, terminal deoxynucleotidyl transferase-mediated dUTP nick end labeling assay; IHC, immunohistochemistry; MD, mean difference; NRE, negative regulatory element; HPV, human papillomavirus; MKK, MAPK kinase; MKKK, MAPK kinase kinase; DAB, 3,3′-diaminobenzidine; CI, confidence interval; HPF, high power field.

cells, such as mouse fibroblasts, induces oncogenic transformation (17). There is strong evidence that the transformation activity of c-mos, like many other oncogene products, is exerted when it is expressed in the G_1 phase. c-mos has been proposed to act as a mitogenic stimulus by modulating, via the MAPK pathway, the activities of many downstream G_1 targets including c-*fos*, c-*jun*, c-*myc*, S6 kinase II, and TCF/Elk-1 (14, 18 and references therein). It has been suggested that c-fos is the main effector of the c-mos/MAPK pathway leading to cellular transformation (14, 19). Furthermore, two recent studies (20, 21) showed that serum-starved *v-mos*-transformed cells had elevated levels of certain cyclins (D, E, and A), cyclin dependent kinases ($p33^{cdk2}$ and $p43^{cdc2}$), and S-phase specific E2F complexes, suggesting that the inability to down-regulate these critical cell cycle regulatory molecules may contribute to neoplastic transformation. Interestingly, it seems that the role of c-mos in somatic cell transformation is not limited only to the G_1 phase but involves mitosis as well. The effects of c-mos in the M phase are characterized by meiotic-like modifications that lead to the production of binucleated cells and may indicate a novel mechanism of CIN (22).

In view of the diverse activities of c-mos in various cell lines and its apparent link with p53, we examined in a series of 56 NSCLCs, which have been used in previous analyses of a G_1 phase protein network (22), the following: *a*) the status of c-*mos* at the protein, mRNA, and DNA levels; *b*) its relationship to genomic instability (aneuploidy) and the kinetic parameters of the tumors (PI and AI); and *c*) its association with p53 alterations and their concomitant relationship with the above parameters. To the best of our knowledge this information has not been addressed thus far.

MATERIALS AND METHODS

Tissue Samples

A total of 56 NSCLCs and adjacent normal lung tissue were analyzed. These tumors were part of a panel of 68 NSCLCs, classified according to the WHO criteria and Tumor-Node-Metastasis system (23), previously investigated for a G_1 phase protein network including p53 (Ref. 24; Table 1).

IHC

Antibodies

For immunohistochemical analysis, the following antibodies were used: P-19 (class, IgG goat polyclonal; epitope, COOH terminus of human c-mos; Santa Cruz, Bioanalytica, Greece); DO7 (class, IgG2b, mouse monoclonal; epitope, residues 1–45 of p53; Dako, Kalifronas, Greece); MIB-1 (class, IgG1, mouse monoclonal; epitope, Ki-67 nuclear antigen; Oncogene Science, Biodynamics, Greece); and p-ERK/E-4 (class, IgG 2a mouse monoclonal; epitope corresponding to the amino acid sequence containing the phosphorylated Tyr 204 of ERK1/2).

Method

IHC was performed by an indirect streptavidin-biotin-peroxidase method, as described previously (23).

Controls

The human cervical cell line ME180 was used as positive control for c-mos expression (16). In addition, the specificity of P-19 anti-mos antibody was tested by preincubating the latter with the appropriate control peptide (Santa Cruz, Bioanalytica). Elimination of immunostaining verified c-mos specificity. Lung carcinoma specimens from our previous study (23), with well-characterized p53 status, were used as controls for p53 protein reactivity. The DB lymphoma c-mos negative cell line (16) was used as a negative control. The specificity of E-4 anti-p-ERK antibody was tested by preincubating the latter with the appropriate control peptide (Santa Cruz, Bioanalytica). Elimination of immunostaining verified p-ERK specificity. Furthermore, in each set of immunoreactions antibody of the corresponding IgG fraction, but of unrelated specificity was used as a negative control.

Evaluation

c-mos. Cytoplasmic and membranous immunoreactivity was considered to be evidence of c-mos expression. Nuclear staining in the presence of cytoplasmic and/or membranous reactivity was also regarded as specific, as described previously (25). Sole nuclear staining was disregarded. IHC was evaluated by examining all of the discreet areas of each tumor specimen. Tumors were considered c-mos(P) when >30% of the tumor cells were stained; otherwise, they were scored negative (N). In a recent immunohistochemical study, we divided the positively stained tumors in two groups: (+), <30%; and (2+), >30% (26). However, for the present study, the criteria were reassessed because only the carcinomas, in which >30% of the cells showed immunoreactivity, were associated with increased c-*mos* mRNA levels.

p53. Tumors were considered positive when >20% of tumor cells showed nuclear staining; otherwise, they were scored as negative.

p-ERK1/2. Tumor cells were evaluated as positive when staining was mainly nuclear because activated ERK translocates to the nucleus to gain access to its transcription factor substrates (18).

Ki-67. Tumor cells were evaluated as positive when nuclear staining, without cytoplasmic background, was observed. The PI was calculated as the percentage of MIB-1 positive cells in five to seven HPFs (at least 1000 cells were assessed). Slide examination was made by three independent observers (V. G. G., P. F., and P. Z.). Interobserver variability was minimal ($P < 0.001$).

Microdissection and Extraction of Nucleic Acids

Microdissection

For DNA extraction, contiguous 5-μm sections were microdissected as described previously (23).

DNA Extraction

DNA was extracted from 50μg of neoplastic material using the phenol/chloroform/isoamylalcohol method (27).

RNA Extraction

Cancerous material with >90% tumor cells was used for RNA extraction, because microdissection is not suitable for RNA handling methods. RNA was extracted by Trizol reagent (Life Technologies, Inc., AntiSel, Greece) according to the manufacturer's instructions.

Multiplex RT-PCR

To examine the mRNA levels of c-*mos* in tumor and adjacent normal tissues, we performed a semiquantitative multiplex RT-PCR method, as described previously (28). Briefly, target mRNA fragment is coamplified with a larger reference mRNA fragment of a ubiquitously expressed molecule. The relative ratios of the amplification products in the tumor samples reflect the relative proportion of input mRNAs and are compared with the relative ratios in the corresponding normal tissue.

Primers

The primers used in the reaction were the following: target cDNA, the amplimers for the c-*mos* fragment were 5′-GCC TGC TCT TCC

Table 1 *Summary of clinicopathological features, p53 and c-mos status, PI, AI, and ploidy status*

				c-*mos* status							p53 status									Clinicopathological features			
Sample	Sex	Age	Smoking	IHC	mRNA expression	DNA amplification	SSCP analysis	Gene mutation	Amino acid substitution	AIm *D8S285*	IHC[a]	SSCP analysis	Defective exon	Gene mutation[a]	Amino acid substitution	AIm *D17S179E*	AI %	PI %	Ploidy	Histology	LN	Stage	Duration of follow up[b]
3	M	61	Yes	N	NE	−	−			ho	N	−					1,6	28,3	A	SQ	No	I	37+
19	M	70	Yes	N[c]	NE	−	−			H	N	−				ho	10,6	NI	D	AD	No	I	34+
20	M	66	Yes	N	NE	−	−			LOH	N	+	9	Not examined		NI	3,5	24,6	D	SQ	No	I	34+
22	M	70	Yes	N[d]	NE	−	−			H	N	−					1,5	46,6	D	AD	No	I	34+
23	M	79	Yes	N	NE	−	−			H	N	−				H	2,6	26,7	D	AD	Yes	II	18
25	M	63	No	N	NE	−	−			H	N	−				ho	1,4	21,3	D	AD	No	I	33+
27	M	70	No	N	NE	−	−			H	N	+	8	Codon 282, CGG → GG	FS	LOH	3,5	13,3	NI	AD	Yes	I	14
30	M	75	Yes	N[d]	NE	−	−			H	N	−					3	28,8	D	UL	No	I	32+
31	M	64	Yes	N	NE	−	+	codon 22, CGG → CTT	R → L	H	N	−				ho	0,6	21,2	D	AD	No	I	10
39	M	56	Yes	N	NE	−	−				N	−				ho	0,9	54,0	D	SQ	Yes	III	9
44	M	72	No	N[d]	NE	−	−			LOH	N	+	6	Codon 213, CGA → GA	FS	ho	0,7	22,3	A	AD	Yes	III	14
45	M	57	Yes	N[d]	NE	−	−			H	N	−				ho	8,9	32,9	D	AD	Yes	II	27
46	M	68	No	N	NE	−	−			LOH	N	−				ho	NI	NI	D	AD	No	I	29+
49	M	53	No	N	NE	−	−			H	N	−					NI	36,9	D	AD	No	I	29+
50	M	62	No	N[d]	NE	−	−			H	N	−				H	1,4	18,1	D	AD	Yes	II	27
51	M	48	Yes	N	NE	−	−			H	N	−				H	2,2	20,0	D	AD	Yes	II	15
54	M	65	Yes	N[d]	NE	−	−			H	N	−				LOH	3,1	32,2	NI	SQ	No	I	28+
62	M	57	Yes	N	NE	−	−			H	N	+	8	Codon 270, TTT → ATT	F → F	LOH	1,5	41,4	A	SQ	No	I	13
66	M	58	Yes	N[d]	NE	−	−			H	N	−				LOH	2,3	33,3	A	SQ	Yes	II	3
13	M	64	Yes	N	NE	−	−			H	P	+	7	Codon 248 CGG → CTG	R → L	ho	NI	32,8	D	SQ	Yes	III	8
15	M	69	Yes	N[d]	NE	−	−			LOH	P	+	5	Codon 163, TAC → TGC	Y → C	LOH	1,1	40,6	A	SQ	No	I	34+
18	M	73	Yes	N	NE	−	−			H	P	+	7	Codon 230, ACC → AAC	T → N	LOH	4,8	43,6	D	SQ	Yes	II	11
24	M	62	Yes	N[d]	NE	−	−				P	+	4	Codon 74, GCC → ACC	A → T	LOH	0,8	26,7	NI	SQ	No	I	N/A
28	M	60	Yes	N	NE	−	−			H	P	+	5	Codon 157, GTC → TCC	V → F	ho	1,4	40,9	A	SQ	No	I	33+
29	M	61	Yes	N	NE	−	−			H	P	+	4	Codon 69, GCT → GGT	A → G	ho	0,3	43,4	A	UL	Yes	III	0
42	M	76	Yes	N	NE	−	−			H	P	+	5	Codon 157, GTC → TTC	V → F	NI	0,6	43,8	A	SQ	Yes	III	30+
47	M	71	Yes	N	NE	−	−			ho	P	−				ho	0,6	54,4	A	SQ	No	I	25
52	M	72	Yes	N	NE	−	−			H	P	+	8	Codon 273, CGT → CAT	R → H	LOH	0,6	39,0	A	SQ	No	III	29+
53	M	60	Yes	N	NE	−	−			H	P	+	9	Codon 319, AAG → AAT	K → N	ho	2,6	51,2	A	SQ	Yes	III	15
55	M	52	No	N	NE	−	−			H	P	+	8	Codon 275, TGT → TTT	C → F	ho	0,8	43,3	A	AD	Yes	II	10
57	M	58	Yes	N	NE	−	−			H	P	+	5	Codon 153, CCC → CAC	P → H	NI	1,8	40,0	A	SQ	Yes	III	8
59	M	65	Yes	N[d]	NE	−	−			H	P	+	5	Codon 143, GTG → GCC	V → A	LOH	NI	30,4	A	AD	No	I	25
60	M	64	Yes	N	NE	−	−				P	−				H	1	38,6	A	AD	Yes	III	23
61	M	59	Yes	N	NE	−	−			H	P	−				LOH	1,1	24,5	D	AD	Yes	III	26+
63	F	60	Yes	N	NE	−	−			H	P	−					1	50,6	A	AD	No	III	25+
64	M	62	Yes	N	NE	−	−			H	P	−				LOH	1,6	39,3	D	AD	No	I	25+
65	M	56	Yes	N	NE	−	−			H	P	−				LOH	0,7	70,4	A	SQ	Yes	II	22
67	M	71	No	N	NE	−	−			H	P	−				ho	0,6	20,2	D	AD	No	I	24+
37	M	71	No	P[d]	OE	−	−			NI	N	−				NI	3,2	28,9	A	AD	Yes	II	12
43	M	60	No	P[d]	OE	−	+	Codon 260, GCC → GCA	A → A	H	N	+	4	Codon 60, CCA → CCT	P → P		3,5	21,4	A	AD	Yes	II	30+
4	M	60	Yes	P[d]	OE	−	−			H	P	+	7	Codon 249, AGG → AGT	R → S	ho	NI	NI	A	UL	No	I	0
9	M	53	Yes	P[d]	OE	−	−				P	+	7	Codon 238, TGT → TTT	C → F	ho	2	30,3	D	AD	No	I	35+
10	F	68	Yes	P[d]	OE	−	−			H	P	+	4	Codon 93, CTG → ATG	L → M	ho	1,8	40,6	A	UL	Yes	II	9
11	M	70	Yes	P[d]	OE	−	−			NI	P	+	8	Codon 280, AGA → ATA	R → I	H	0,7	36,0	A	SQ	No	I	34+
14	M	74	Yes	P[d]	OE	−	−			H	P	+	7	Codon 239, AAC → ACC	N → T	ho	1,3	38,5	A	SQ	Yes	III	8
16	M	63	Yes	P[d]	OE	−	−			H	P	−				NI	0,8	4,6	D	AD	No	I	7
17	M	64	Yes	P[d]	OE	−	−			H	P	−				H	1,2	27,3	NI	SQ	No	II	34+
26	M	63	Yes	P[d]	OE	−	−			H	P	+	6	Codon 196, CGA → CCA	R → P		0,1	29,2	A	AD	Yes	II	17
48	M	73	Yes	P	OE	−	+	Codon 324, AGC → AGT	S → S	H	P	+	7	Codon 237, ATG → ATA	M → I		0,5	44,0	D	SQ	No	III	14
56	M	58	Yes	P	OE	−	−			H	P	−				ho	0,4	47,3	A	SQ	Yes	II	11
58	M	52	No	P	OE	−	−			H	P	−				ho	0,6	46,0	A	AD	Yes	II	26+
68	M	61	Yes	P	OE	−	−			H	P	−				P	2,1	59,1	A	SQ	Yes	II	21
1	M	57	Yes	NI	NI	−	−			H	P	−				H	4,8	31,1	A	AD	Yes	III	3
2	M	60	Yes	NI	OE	−	−			H	NI	−				LOH	NI	NI	NI	SQ	Yes	III	21
7	M	64	Yes	NI	NI	−	−			H	P	+	8	Codon 273, CGT → CTT	R → L	ho	1,2	27,2	A	SQ	Yes	II	35+
21	M	70	Yes	NI	NI	−	−				N	−				LOH	NI	34,5	D	SQ	Yes	III	1

[a] Data obtained from previous study (23).

[b] In months after surgery, (+) indicates that the patient is alive.

[c] N, negative; P, positive; NI, noninformative; NE, normal expression; OE, over expression; +, possible mutation; −, no mutation; FS, frameshift; H, heterozygous; ho, homozygous; D, diploid; A, aneuploid; SQ, squamous cell carcinoma; AD, adenocarcinoma; UL, undifferentiated large cell carcinoma; LN, lymph node invasion.

[d] Indicates samples examined for ERK activity.

TCC ACT CG-3′ (pos. 803) and 5′-AGT ATG TGC TGC CGC TCC CC-3′ (pos. 1100); reference cDNA, a 548-bp *β-actin* fragment was used as reference.

Controls

Because the c-*mos* gene is intronless, a positive PCR product could theoretically be obtained from DNA contaminating the RNA solutions. To exclude the latter possibility, we performed the reactions in the presence or the absence of reverse transcriptase before cDNA amplification. Contaminated RNA solutions were treated with DNase and/or 4 M $LiCl_2$ and tested again as described above. To exclude the possibility of having false-positive results attributable to a carry-over effect in our assay, RNA was isolated from several murine cell lines and included in the experiments as negative controls. Because the primers used do not share sequence homology with murine c-*mos* (12, 29), no specific PCR product was expected in the murine cells tested in the absence of human c-*mos* sequence contamination. To avoid possible RT-PCR intra-assay alterations that could affect the original transcript ratio (target *versus* reference), 2-fold serial dilutions of RNA solutions were used in control amplifications. From these reactions a low number of PCR cycles was established for assessing RNA transcript ratios.

Evaluation

The relative ratio of c-*mos*:*β-actin* was quantified using an image analysis system (Media Cybernetics, Silver Spring, Maryland). Because *β-actin* amplification is not necessarily similar to that of c-*mos*, comparison of the relative ratio of c-*mos* and *β-actin* between corresponding tumor and normal specimens was performed [c-*mos*/*β-actin* (tumor):c-*mos*/*β-actin*(normal)]. Performing the above procedure in 100 pairs of normal-normal specimens to determine the normal variability of this ratio, we found it to be 1.00 ± 0.18. When the tumor:normal relative ratio was within this range, c-*mos* mRNA levels were considered to be normal. Values higher than 1.18 were interpreted as c-*mos* mRNA overexpression. All of the reactions were performed twice.

Northern Blot Analysis

Thirty μg of RNA were electrophoretically separated on 1% 4-morpholinepropanesulfonic acid-formaldehyde gel and transferred to nylon membrane by capillary blotting. Equal loading was confirmed by staining with ethidium bromide. Hybridization was performed with a 40-bp antisense c-*mos* 3′end-labeled FITC-conjugated dUTP probe spanning nucleotides 1061–1100 of the published cDNA sequence (12). The probe was labeled using the enhanced chemiluminescence 3′-oligolabeling and detection system (Amersham Life Science, Buckinghamshire, England). The filter was prehybridized in the buffer supplied by the manufacturer at 42°C for at least 2 h and hybridized at 42°C for 12 h in the same buffer that contained the c-*mos* 3′end FITC-dUTP-labeled probe. The membrane was washed, twice with 5× SSC-0.1% SDS at 42°C for 5 min, once with 1× SSC-0.1% SDS at room temperature for 5 min, and once with 0.1× SSC-0.1% SDS at room temperature for 5 min. For detection, the appropriate anti-FITC antibody was applied and c-*mos* mRNA expression was analyzed using an enhanced chemiluminescence system (Amersham Corp., Arlington Heights, IL). RNA from the ME180 and the DB cell lines were used as c-*mos* positive and negative controls, respectively.

D-PCR

To examine amplification of the c-*mos* gene in tumor tissues, we performed the D-PCR method as described previously (30). Briefly, this technique is based on the coamplification of a target DNA fragment with a shorter reference DNA fragment of a single-copy gene. The relative ratios of the amplification products in the tumor samples reflect the relative proportion of DNA fragments and were compared with the relative ratios in the adjacent normal tissue. It should be noted that theoretically the tumor:normal relative ratio in normal tissue equals 1, because normally no gene amplification occurs.

Primers

We used a 245-bp region of the *IFN-γ* gene as a reference fragment. The sequences of the primers used to amplify the fragment were as follows: 5′ ACA AGG CTT TAT CTC AGG GGC CAA C 3′ (pos. 4972) and 5′ AAG CAC CAG GCA TGA AAT CTC C 3′ (pos. 5195). The target DNA sequence was the c-*mos* fragment identical to that amplified in the Multiplex RT-PCR assay described above.

Evaluation

The relative ratio of c-*mos*:*IFNγ* was quantified using an image analysis system (Media Cybernetics). Values >2 were regarded as indicative of c-*mos* gene amplification.

SSCP

The method was performed on matched normal and tumor DNA as described previously (23). On the basis of the nucleotide sequence of the c-*mos* gene reported by Watson *et al.* (12), amplimers were designed using the Oligo software (version 4.01; National Biosciences, Inc., Plymouth, MN) to produce four partially overlapping fragments (Fig. 1): fragment 1, 5′ GTC TCT TCA TTC ACT CCA GCG 3′ (pos: 194) and 5′ CTT GTT CAC TTG CTT TAT GGC 3′ (pos: 515); fragment 2, 5′ TGG GAG CTG GAG GGT TTG GC 3′ (pos: 438) and 5′ TCC AGT GCG GCA GTG AGG CT 3′ (pos: 750); fragment 3, 5′ GCC TGC TCT TCC TCC ACT CG 3′ (pos: 803) and 5′ AGT ATG TGC TGC CGC TCC CC 3′ (pos: 1100); and fragment 4, 5′ AAA TGA CTA CCA AGC AGG CG 3′ (pos: 1052) and 5′ ACC AAG TTT TCA GTC AGC CG 3′ (pos: 1284). The amplimers for p53 have been reported previously (23).

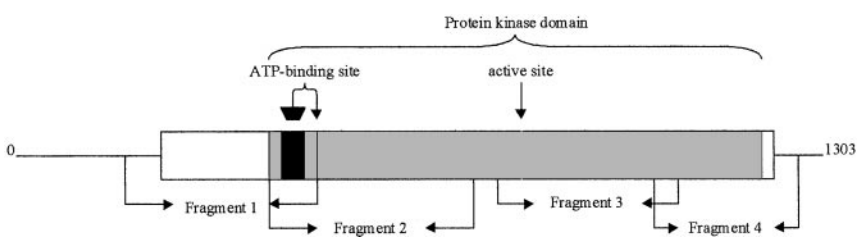

Fig. 1. Schematic representation of the c-*mos* cDNA. The amplimers used in mutation analysis are marked down.

Table 2 *Association between c-mos, p53, c-mos/p53 patterns and clinicopathological features, PI, AI, and ploidy status*

Expression		Smoking history			Histology				Lymph node invasion			Stage				PI			AI			Ploidy status		
		Yes	No	*P*	Sq[a]	Ad	UL	*P*	+	−	*P*	I	II	III	*P*	mean (n)	SD	*P*	mean (n)	SD	*P*	A	D	*P*
c-mos IHC	N	30	8	0.625	17	19	2	0.549	18	20	0.755	19	8	11	0.043	35.75 (36)	12.01	0.874	1.965 (34)	2.348	0.208	17	18	0.152
	P	11	3		6	6	2		8	6		4	8	2		34.99 (13)	13.37		1.539 (13)	1.224		10	3	
p53 IHC	N	14	8	**0.013**[b]	7	14	1	0.549	11	11	0.788	12	7	3	0.140	29.336 (20)	10.044	**0.004**	3.192 (19)	2.58	**<0.001**	6	14	**0.005**
	P	30	3		18	12	3		18	15		11	10	12		38.641 (32)	12.134		1.306 (30)	1.119		23	8	
c-mos/p53	N/N	13	6	**0.011**	6	12	1	0.300	8	11	0.471	12	5	2	**0.018**	29.54 (17)	10.68	**0.022**	3.170 (17)	2.736	**0.001**	4	13	**0.007**
	P/N	0	2		0	2	0		2	0		0	2	0		25.21 (2)	5.34		3.379 (2)	0.229		2	0	
	N/P	17	2		11	7	1		10	9		7	3	9		40.77 (19)	11.47		1.268 (17)	1.069		13	5	
	P/P	11	1		6	4	2		6	6		4	6	2		36.62 (11)	14.10		1.049 (11)	0.689		8	3	

[a] Sq, squamous cell carcinoma; Ad, adenocarcinoma; UL, undifferentiated large cell carcinoma; N, negative; P, positive; D, diploid; A, aneuploid.
[b] Bold indicates statistically significant values.

Automated Sequencing

The DNA fragments that showed mobility shifts were purified using the QIA Gel Extraction kit (Qiagen, Bioanalytica, Greece) and analyzed further with automated sequencing. Cycle sequencing for c-*mos* was performed on Gene Amp PCR system 9700 (PE-Applied Biosystems, Warrington, United Kingdom) using the ABI PRISM BigDye Terminator Cycle Sequencing Kit (PE-Applied Biosystems) according to the manufacturer's directions. In brief, 100 ng of purified DNA were mixed with 1.6 pmol of each primer, 0.75 μl of BigDye mixture, and 3.25 μl of the Diluent solution in a 10-μl reaction. The thermal profile of the reaction comprised: 1 min at 95°C, 25 cycles of 20 s at 95°C, 15 s at 58°C, 30 s at 68°C, and 3 min 30 s at 60°C, followed by a final extension at 60°C for 5 min. The products were electrophoresed in a denaturing gel on an ABI PRISM 377 DNA Sequencer (PE-Applied Biosystems). Results were analyzed using the Genescan and Genotyper software (PE-Applied Biosystems). The *p53* exons that harbored putative mutations were amplified with primers tailed with M13 forward and reverse primers and sequenced as formerly described (23). All of the PCR and sequencing reactions were performed and confirmed twice by two independent laboratories.

AIm Analysis

To examine allelic alterations of c-*mos* and *p53*, we chose two markers: *D8S285*, which lies within the vicinity (telomeric boundary) of c-*mos*, and *D17S179E*, a pentanucleotide marker located within the first intron of *p53*. Primers were designed using the Oligo software (version 4.01; National Biosciences, Inc.).

Primers

The primers were: *D17S179E*, 5′-AGTAAGCGGAGATAGTGCCA-3′ (ABI-HEX labeled) and 5′-GCACTGACAAAACATCCCCT-3′; and *D8S285*, 5′-CAGAATCTTTGCTACCTACA-3′ and 5′-CAGTTTTTATGGGTTTATGG-3′.

Method

The reaction mixture consisted of: 1× GeneAmp buffer II, 250 μM deoxynucleotide triphosphates, 2 mM $MgCl_2$, 0.25 μM of each primer, and 2 units of AmpliTaq Gold polymerase. The PCR amplification parameters were: initial denaturation for 12 min at 95°C, 30 cycles of 30 s at 94°C, 30 s at 55°C, and 30 s at 72°C, followed by a final extension of 20 min at 72°C. The *D17S179E* products were analyzed on an ABI-PRISM 377 Automatic Sequencer (PE-Applied Biosystems). The products of *D8S285* were analyzed on 10% native gels and stained with silver, and results were evaluated by densitometry. All of the LOH results were confirmed with a second PCR.

Evaluation

The variability of the reaction and the establishment of the cutoff level for scoring AIm have been described previously (31). Briefly, when the allele ratio values were $\leq$0.65 or $\geq$1.54, samples were scored as LOH; whereas when their values covered the range 0.77–1.23, they were scored negative.

Nuclear DNA Ploidy Analysis

The samples were stained according to the Thionin-Feulgen procedure (32). The measuring and evaluation procedures have been reported formerly (28, 33). Cases with >5% of cells with DNA content above the 5c limit were considered as aneuploid (33).

TUNEL

Method

Double-strand DNA breaks were detected by TUNEL according to the method of Gavrieli *et al.* (34).

Controls

We used tissue sections incubated with DNase I before treatment with terminal deoxynucleotidyltransferase as positive controls and sections incubated in terminal deoxynucleotidyltransferase buffer without the presence of the enzyme as negative controls.

Evaluation

Cells were considered to undergo apoptosis when nuclear staining, without cytoplasmic background, was observed. AI was estimated as the percentage of apoptotic cells in 10 HPFs (counted cells, 900–10,000). Slide examination was performed by three independent observers (P. F., V. G. G., P. Z.). Interobserver variability was minimal ($P < 0.001$).

Statistical Analysis

The possible associations between c-mos and p53 status independently, c-mos/p53 patterns with PI, logAI, ploidy status, and clinicopathological parameters were assessed with the nonparametric Kruskal-Wallis and Pearson χ^2 tests (Table 2). Furthermore, ANOVA was used to evaluate more specifically the possible association between p53 status, c-mos/p53 patterns, and PI and logAI (Table 3). Logistic regression model formulation was applied for estimating possible associations between p53 status, c-mos/p53 patterns, and ploidy status (Table 3). Finally, Kaplan-Meier survival curves were plotted for the parameters examined in the present study. Differences between survival curves were examined by log-rank testing. All of the

Table 3 *Association between PI, logAI, ploidy, and p53, c-mos/p53 patterns*

c-mos is not correlated with any of the examined parameters.

	ANOVA				Logistic regression analysis	
	PI		logAI		Ploidy	
	MD (95% CI)	*P*	MD (95% CI)	*P*	Odds ratio (95% CI)	*P*
Intercept	29.34 (24.22, 34.45)	<0.001	0.921 (0.579, 1.262)	**<0.001**		0.083
p53(P)[a]	9.31 (2.79–15.82)	**0.006**[b]	−0.934 (−1.371, −0.498)	**<0.001**	6.708 (1.923–23.409)	**0.003**
p53(N)						
Intercept	29.53 (23.83, 35.22)	**<0.001**	0.886 (0.532, 1.240)	**<0.001**		**0.039**
c-mos(P)/p53(P)	7.25 (−1.83, 16.33)	0.115	−1.099 (−1.663, −0.534)	**<0.001**	8.667 (1.526–49.220)	**0.015**
c-mos(N)/p53(P)	11.20 (3.36, 19.03)	**0.006**	−0.877 (−1.378, −0.377)	**0.001**	8.450 (1.843–38.753)	**0.006**
c-mos(P)/p53(N)	−4.38 (−21.92, 13.17)	0.618	0.331 (−0.760, 1.421)	0.544	4360 (0.000–5.110E+25)	0.747
c-mos(N)/p53(N)						

[a] P, positive; N, negative.
[b] Bold indicates statistically significant values.

analysis was performed with the SAS statistical package. The statistical difference was considered significant when the *P* was <0.05.

RESULTS

c-mos and p53 Analysis

c-mos Status

IHC and Relationship with Clinicopathological Parameters. Expression of c-mos was observed in 14 of 52 informative cases (27%). Staining was mainly cytoplasmic and membranous, but in certain cases nuclei reacted with the anti-mos antibody as well. Expression was confined to the cancerous areas (Fig. 2*a*). Considerable intratumor staining heterogeneity was noticed. The relationship between c-mos immunohistochemical status, smoking habits, histology, lymph node status, and stage is presented in Table 2. Statistical analysis revealed an association between c-mos expression and stages grouped as I and II/III [4 of 23 (17.4%) *versus* 10 of 29 (34%); $P = 0.018$ by Pearson χ^2; Table 2].

c-mos mRNA Analysis. The c-*mos* mRNA levels were examined in normal and tumor paired samples by a semiquantitative multiplex RT-PCR assay. Interestingly, c-*mos* mRNA was detected in all of the normal and tumor specimens including the cell lines used as negative controls in IHC analysis. The possibility of false positive results was excluded by using the appropriate controls (see "Materials and Methods"). However, multiplex RT-PCR revealed in 15 of 53 informative cases (28%) significantly higher levels of c-*mos* mRNA in the tumors compared with the corresponding normal tissues (Table 1; Fig. 3). In these samples, the relative ratio ranged between 3 and 7.2 compared with the value 1.00 (±0.18) characteristic of the normal status (see "Materials and Methods"). It is of the most interest that complete concordance was found between c-mos immunohistochemical positivity and c-*mos* mRNA overexpression (Table 1). Furthermore, RNA from six matched normal-tumor cases (17, 26, 48, 56, 58, and 68) with c-mos protein expression was available for Northern blot analysis. The levels of c-*mos* mRNA were higher in the tumor samples than in the corresponding normal ones, which confirms the multiplex RT-PCR results. Two c-*mos* transcripts of 3.5 and 1.7 kb were clearly detected in two tumor samples, whereas in the other four cancerous ones only the 3.5 kb band was definite. All of the normal counterparts expressed the 3.5 kb transcript (Fig. 4).

c-*mos* Gene Alterations. Three of the 56 samples (5%) showed tumor-specific mobility shifts (Fig. 5). Sequence analysis revealed one missense mutation and two silent ones. The missense mutation resulted in a single-base substitution of arginine (R) to leucine (L; CGG→ CTT) at codon 22 (case 31), whereas the silent mutations resulted in an alanine (A) substitution (GCC→GCA) at codon 260 (case 43) and in serine (S) substitution (AGC→AGT) at codon 324 (case 48; Table 1). D-PCR in our series did not reveal any c-*mos* gene amplification. Given the latter, the observed AIm in 4 of 47 informative cases possibly reflects LOH at the chromosomal locus *D8S285* (Fig. 6*a*), which lies at the telomeric boundary of c-*mos* (Table 1).

Relationship between c-mos Expression and PhosphoMAPK Staining. To examine the downstream biochemical effect of c-mos expression, we performed an immunohistochemical analysis of phosphorylated ERK1/2 in a group of c-mos positive and c-mos negative cases (Table 1). Staining was mainly nuclear (Fig. 2*b*). Expression was observed in the cancerous areas and in the surrounding normal tissues as well. We did not detect any differences in ERK1/2 staining among the c-mos(P) and c-mos(N) group of patients.

p53 Status

IHC and Relationship with Clinicopathological Parameters. Expression of p53 was observed in 33 of 55 informative cases (60%). The association of p53 with the clinicopathological parameters of the patients is summarized in Table 2. A significant association was noticed between p53 positive staining and smoking [30 of 44 (68%) *versus* 3 of 11 (27%); $P = 0.013$ by Pearson χ^2; Table 2; and $P = 0.020$; odds ratio, 5.714 (1.313–24.871) by logistic regression analysis].

***p53* Gene Alterations.** Sequence analysis revealed *p53* mutations in 24 of 56 cases (43%). Twenty mutations were missense, two were silent (cases 43 and 62), and two were frameshift (cases 27 and 44; Table 1). One more sample (case 20) yielded a tumor-specific mobility shift on SSCP analysis, but further sequencing was not performed because material was not available. A highly significant association was observed between *p53* gene mutations and p53 immunostaining [20 of 33 (61%) *versus* 4 of 22 (18%); $P = 0.005$ by Pearson χ^2]. AIm analysis with *D17S179E* (Fig. 6*b*) showed LOH in 14 of 21 informative samples (67%). Seven of these cases (50%) were accompanied by *p53* point mutations in the remaining allele (Table 1). Because the IHC status of p53 is highly correlated with sequence analysis and the number of informative specimens at the *D17S179E* locus was rather low, we decided to consider p53 immunohistochemical positivity as an indicator of *p53* gene alterations for subsequent analyses.

Analysis of Ploidy Status and Tumor Kinetics (Proliferation and Apoptosis): Relationship to the c-mos/p53 Patterns

Ploidy Status and Tumor Kinetics Analysis

Twenty nine of 51 tumors (60.6%) were scored as aneuploid (Fig. 7). No statistically significant association between the ploidy status and the clinicopathological features of the tumors was found. The AI ranged from 0.13% to 10.67% with a mean value 2.037 ± 2.029% (Fig. 8). No significant association was found between AI, smoking,

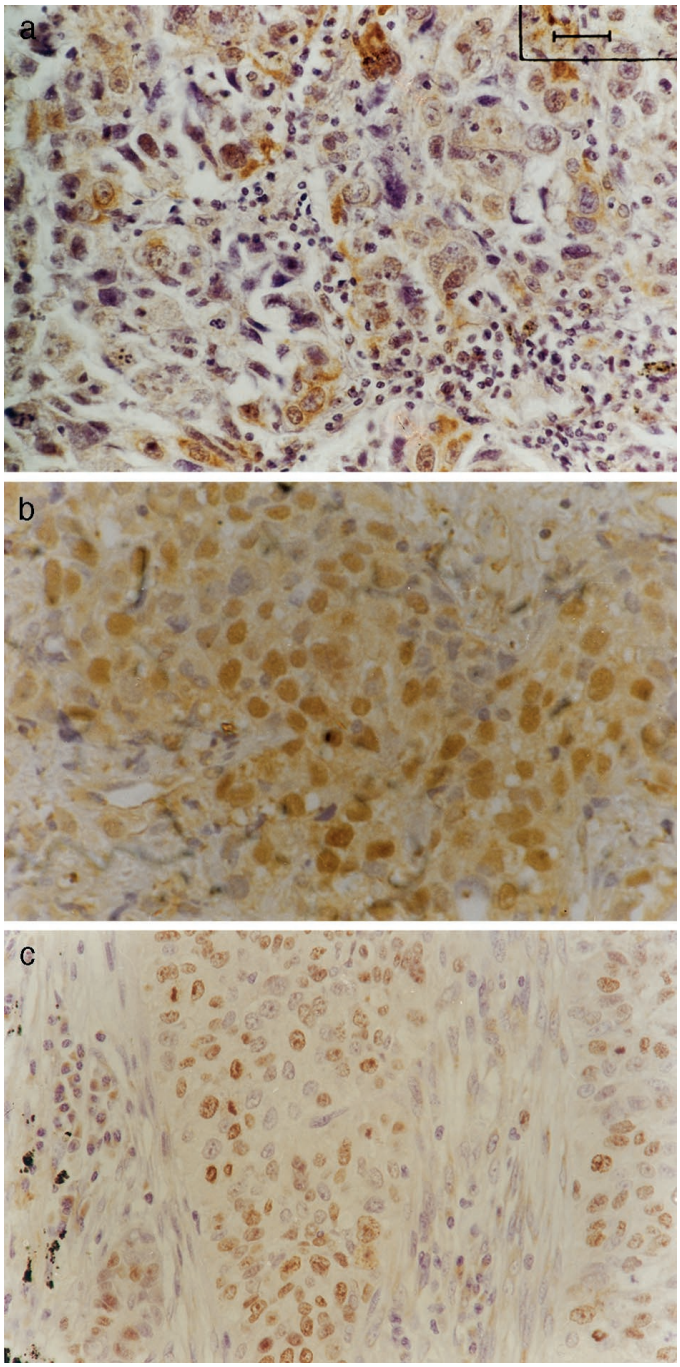

Fig. 2. Representative immunohistochemical results (see "Materials and Methods"); *a*, squamous cell lung carcinoma (case 11) with c-mos overexpression. Streptavidin-biotin peroxidase technique with P19 anti-c-mos antibody (DAB as chromogen) and hematoxylin counterstain (×400). *b*, squamous cell lung carcinoma (case 14) with nuclear localization of activated ERK1/2. Streptavidin-biotin peroxidase technique with E-4 anti-p-ERK antibody (DAB as chromogen) and hematoxylin counterstain (×400). *c*, squamous cell lung carcinoma (case 21) with high proliferative activity (PI = 35%). Streptavidin-biotin peroxidase technique with MIB1 anti-Ki67 antibody (DAB as chromogen) and hematoxylin counterstain (×400).

and the pathological subtype of the carcinomas. In the present study, proliferative activity was reflected by the PI using Ki-67, the most reliable antibody for estimating growth fraction by IHC (35). The percentages of Ki-67 positive cells in the cancerous areas ranged from 6.2 to 70.4%, and the mean PI was 35.06 ± 12.16% (Fig. 2*c*). The PI was significantly higher in squamous cells than adenocarcinoma cells [$P = 0.006$; MD = 9.57 (2.94, 16.21) by ANOVA] and in smokers than nonsmokers [$P = 0.019$ by Kruskal-Wallis test]. The aneuploid tumors demonstrated a significantly higher PI [$P = 0.006$; MD = 9.57 (2.94, 16.21) by ANOVA] and lower AI [$P = 0.031$ by Kruskal-Wallis test and $P = 0.017$; MD of logAI = −0.628 (−1.139, −0.117) by ANOVA] than the diploid ones.

Relation to the c-mos/p53 Patterns

Correlation of c-mos and p53 status independently with ploidy and tumor kinetics showed that the cases with c-mos overexpression were more frequently associated with aneuploidy and appeared to have a lower AI than the c-mos(N) group, but these differences did not reach significance (Tables 2 and 3). Only the p53(P) carcinomas were significantly associated with aneuploidy, increased PI, and decreased AI in comparison with p53(N) cases (Tables 2 and 3).

When c-mos expression was examined in association with p53 status, four c-mos/p53 patterns were observed (Table 2). The most frequent ones were the c-mos(N)/p53(P) and c-mos(N)/p53(N) patterns, with 19 patients (37%) each, followed by the c-mos(P)/p53(P) phenotype that accounted for 12 cases (23%). Pearson χ^2 analysis showed a correlation between c-mos/p53 expression patterns, smoking ($P = 0.011$; Table 2) and disease stage ($P = 0.018$; Table 2). However, these associations were found to be independent associations when the logistic regression model was applied. The c-mos(P)/p53(P) and c-mos(N)/p53(P) phenotypes had significantly lower AI scores and were more frequently associated with aneuploidy than were the c-mos(N)/p53(N) tumors (Table 3; Fig. 9), whereas regarding proliferation, only the c-mos(N)/p53(P) profile showed significantly higher PI values than the c-mos(N)/p53(N) pattern (Table 3; Fig. 9).

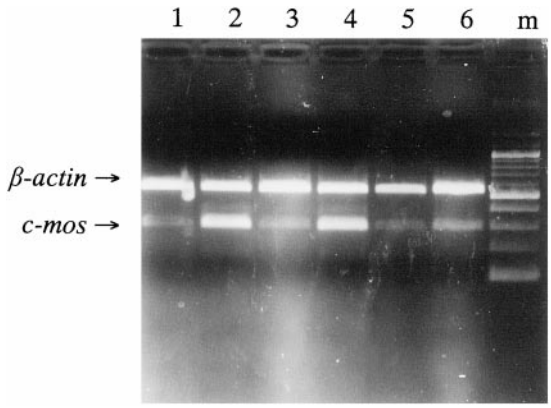

Fig. 3. Representative results of the multiplex RT-PCR for estimating the levels of c-*mos* mRNA; *m*, 100-bp DNA ladder; *Lanes 1* and *2*, and *Lanes 3* and *4*, matched normal-tumor cases (sample 10 and 11, respectively) with c-*mos* mRNA overexpression; *Lanes 5* and *6*, matched normal-tumor case (sample 13) with c-*mos* mRNA normal expression.

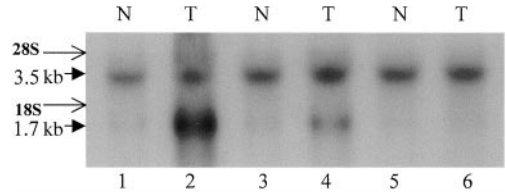

Fig. 4. Representative Northern blot analysis of c-*mos* RNA. Equal loading was confirmed by staining with ethidium bromide; *Lanes 1* and *2*, and *Lanes 3* and *4*, matched normal-tumor cases (sample 17 and 48, respectively) with c-*mos* mRNA overexpression in the tumor sample; *Lanes 5* and *6*, matched normal-tumor case (sample 13) with c-*mos* mRNA normal expression. Two c-*mos* mRNA transcripts of 3.5 and 1.7 kb were detected in tumor cases with c-mos overexpression, whereas only the 3.5 kb message is clear in the tumor sample with normal c-mos status and in all of the normal counterparts.

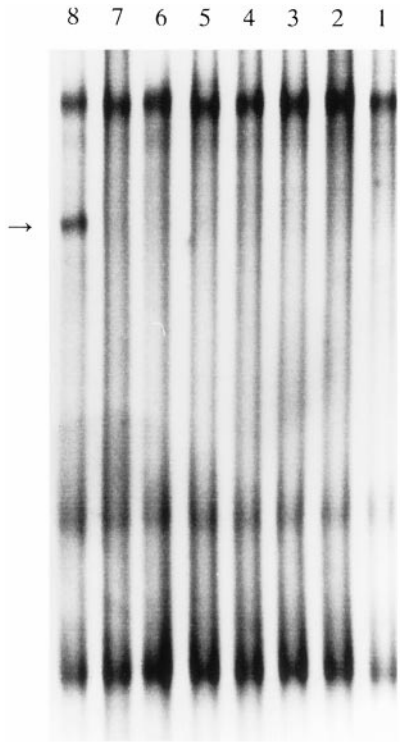

Fig. 5. Representative results of the SSCP analysis for fragment 1 of c-*mos* gene on matched normal-tumor samples (*Lanes 1* and *2*, sample 28; *Lanes 3* and *4*, sample 29; *Lanes 5* and *6*, sample 30; and *Lanes 7* and *8*, sample 31). The differences in the electrophoretic profile of the tumor samples compared with the respective normal ones are marked by the *arrow*.

Survival Analysis

Survival analysis (follow-up duration up to 37 months) using the Kaplan-Meier method did not reveal any statistically significant association between patient outcome, c-mos status, p53 overexpression, and c-mos/p53 patterns.

DISCUSSION

There is little published information on alterations of the constituents of the MAPK cascade in lung cancer (36). We are aware of only one report that has shown low expression of c-mos in mouse lung tissue (37). Our study, which deals with the status of c-*mos* and its relationship with its putative downstream sensor p53, tumor growth parameters, and genomic instability in human NSCLCs, has yielded several novel findings.

Overexpression of c-mos was observed in 27% of the tumors. The observation that staining was restricted mainly to the cytoplasm and membrane of the malignant cells is in accordance with the fact that c-mos is a cytoplasmic serine-threonine kinase (14). However, immunostaining was also noticed in the nuclei of some cancerous cells. The phenomenon of nuclear translocation has been observed with components of the MAPK module and is possibly related to the end result of transcriptional activation (38). Furthermore, Min Wang *et al.* (39) showed that microinjected c-mos in mammalian somatic cells can enter the nucleus and bind to the kinetochores disrupting the normal mitotic progression. Thus, nuclear staining of c-mos may be associated with its ability, demonstrated *in vitro*, to superimpose a meiotic process on the mitotic program of somatic cells, negatively influencing chromosome stability (22). This may be of relevance to our finding that 77% of c-mos positive cases in our series were associated with aneuploidy. Heterogeneous immunoreactivity was also noticed within tumors, possibly reflecting either c-mos cell-cycle fluctuations (16, 40) or clonal expansion of c-mos positive cells, during cancer progression. The higher expression of c-mos protein in stage II/III (34%) than in stage I carcinomas (17.4%; $P = 0.018$) supports the latter view.

The concordance between c-mos immunohistochemical positivity and high c-*mos* mRNA levels along with the absence of gene amplification suggests that its deregulated expression is mainly a consequence of increased transcription. This is an intriguing finding, because normally c-*mos* is specifically transcribed in germ cells and plays a critical role in meiosis, whereas in somatic cells, it is transcriptionally silent or expressed at low levels (16). It has been shown that c-*mos* in somatic cells is suppressed by a NRE, located between 392 and 502 bp upstream from its initiation site (41). A candidate c-*mos* repressor was identified in the nuclear extracts of several somatic cell lines but not in male germ cells in which c-*mos* was transcribed (42). Disruption in the repressor-NRE interaction (*e.g.*, deletion or mutations of the NRE, impaired function, or expression of the repressor) may possibly account for c-*mos* transcriptional activation in our cases. To our knowledge, there is only one previously reported study (43) in primary human tumors, in which detection of c-*mos* mRNA in thyroid carcinomas is described. The authors also observed abnormal transcripts in a medullary thyroid carcinoma (43). However, the lack of internal reference material (adjacent normal thyroid tissue) in that study makes it difficult to judge the role of c-mos in thyroid carcinogenesis. On the other hand, we have clearly demonstrated increased expression of c-mos in lung cancerous tissue compared with adjacent normal tissue. It is noteworthy that the c-*mos* gene shares sequence homology with the HPV *E2* gene, and cross-reactivity of these elements may lead to false-positive results (44). However, we have recently investigated our NSCLC series for HPVs but found no indication of HPV infection (45). Finally, Northern analysis of six cases with c-mos protein overexpression revealed two c-*mos* transcripts of 3.5 and 1.7 kb. The 3.5-kb band was clearly

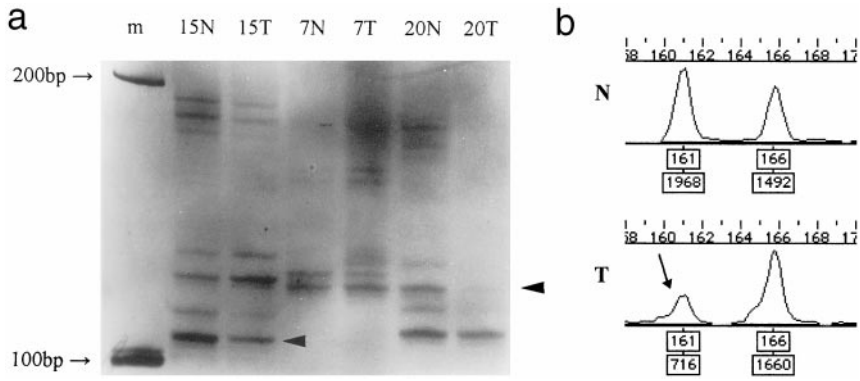

Fig. 6. Representative result of AIm analysis (see "Materials and Methods"); with chromosome marker *D8S285* (silver staining). LOH is indicated by an *arrowhead* (*a*) and *b*, with chromosome marker *D17S179E* (case 54; fluorescence analysis). The *top* numbers in *b* represent the PCR product length, whereas the *bottom* ones demonstrate fluorescence emission intensity. LOH is indicated by an *arrow*; *N*, normal sample; *T*, tumor sample.

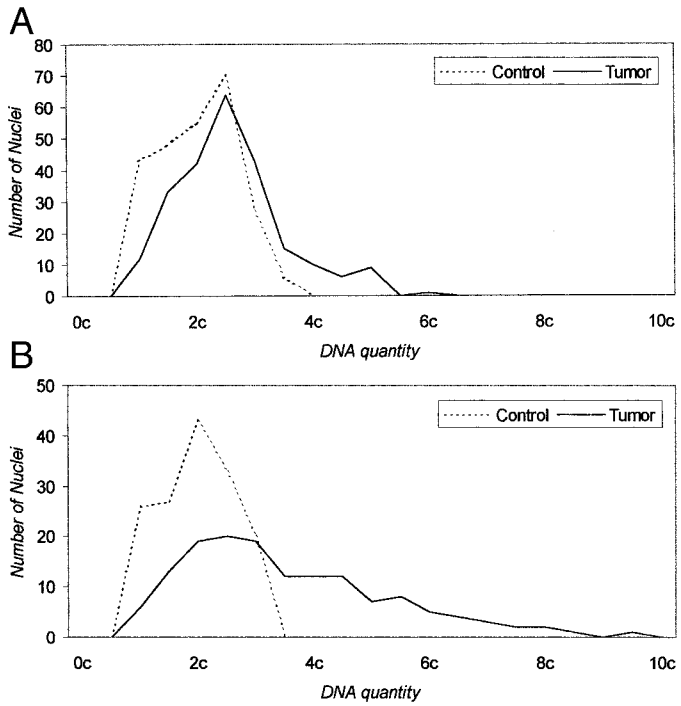

Fig. 7. DNA content of the tumor cells (ploidy analysis; see "Materials and Methods"). *A*, diploid tumor (case 9); *B*, aneupoid tumor (case 10).

detected in all of the matched normal-tumor samples, whereas the 1.7-kb transcript was detected in two tumor samples. This finding is consistent with the report of Li *et al.* (16), who detected similar c-*mos* messages in various cell lines. The significance of these transcripts in c-*mos* regulation remains to be clarified.

At the DNA level, we did not observe amplification of the c-*mos* gene, a finding which is in line with the results of previously published studies in primary NSCLCs (46), NSCLC cell lines (47), head and neck squamous carcinomas (48), and primary gastric carcinomas (49). Structural abnormalities within c-*mos* and its flanking region were detected in pleomorphic adenomas by Stenman *et al.* (50). Restriction fragment analysis indicated that these genetic lesions were the result of multiple subtle mutations rather than rearrangements (50). Sequencing of c-*mos* in our cases showed one missense and two silent point mutations. We did not find the previously reported polymorphism (G to T transversion) at codon 105 (51, 52). The missense mutation observed in case 31 resulted in a R to L substitution at codon 22. Its significance is unclear because c-mos protein in this patient was undetectable and c-*mos* mRNA levels were normal. Codon 22 lies near Ser-3 and Ser-16, the phosphorylation of which is important for c-mos stability (53, 54) and interaction with MKK (55). In addition, Ser-3 is phosphorylated *in vitro* by ERKs, which forms a positive feedback loop (56). Thus, one possibility is that this mutation in the NH_2-terminal region destabilizes c-mos and disrupts the mos-ERK feedback loop, which affects signal transduction through the ERK pathway.

The mos/MKK/ERK pathway is involved in the cellular processes of growth (reviewed in Refs. 14, 38, 40, and 57) and differentiation (58). *In vitro* studies have shown that the exact outcome of this signal transduction pathway [proliferation (reviewed in Refs. 14, 38, 40, and 56), cell cycle arrest (59), apoptosis (59), and differentiation (58)] depends on various parameters, such as the cell type (14, 58), the cell-cycle phase (59), and the levels of c-mos protein (40). This diversity of function is not surprising for MKKKs like c-mos, because unlike MAPKs, which are specifically recognized by their corresponding MKKs, MKKKs interact with a number of MKKs, enabling diversity in the cellular response (38). By taking into account the above apparent opposite actions of c-mos, we were led to investigate its relationship with the tumor kinetic parameters of proliferation and apoptosis. No significant differences were found between the c-mos(P) and the c-mos(N) group of patients (Table 2), which contrasts with the results of Fukasawa *et al.* (59), who reported that elevated c-mos levels lead to apoptosis or cell cycle arrest. One possible explanation for this apparent discrepancy is that in many of our c-mos(P) cases, a downstream inducer of apoptosis may have been defective. Prompted by the recent study of Fukasawa and Vande Woude (11), who showed that c-mos/MKK/ERK-induced apoptosis or growth arrest is p53 dependent, we sought to investigate the relationship between c-mos expression and p53 status and found that c-mos overexpression was indeed frequently accompanied by *p53* alterations (Table 1). Moreover, the fact that the c-mos(P)/p53(P) immunophenotype had significantly lower AI values and was more frequently associated with aneuploidy only from the c-mos(N)/p53(N) profile, but not from the c-mos(N)/p53(P) pattern (Table 3), suggests that p53 status is the main determinant of ploidy status and apoptosis in our series. This finding also strengthens the concept that wt p53 plays a "safeguard" role in preventing oncogene-mediated activation of the mos/MKK/ERK pathway (11). A similar wt p53 "safeguard" function seems to apply to other active oncogenes such as *ras* (5, 60) and *β-catenin* (61). The finding that the group of tumors with *p53* alterations showed increased prolif-

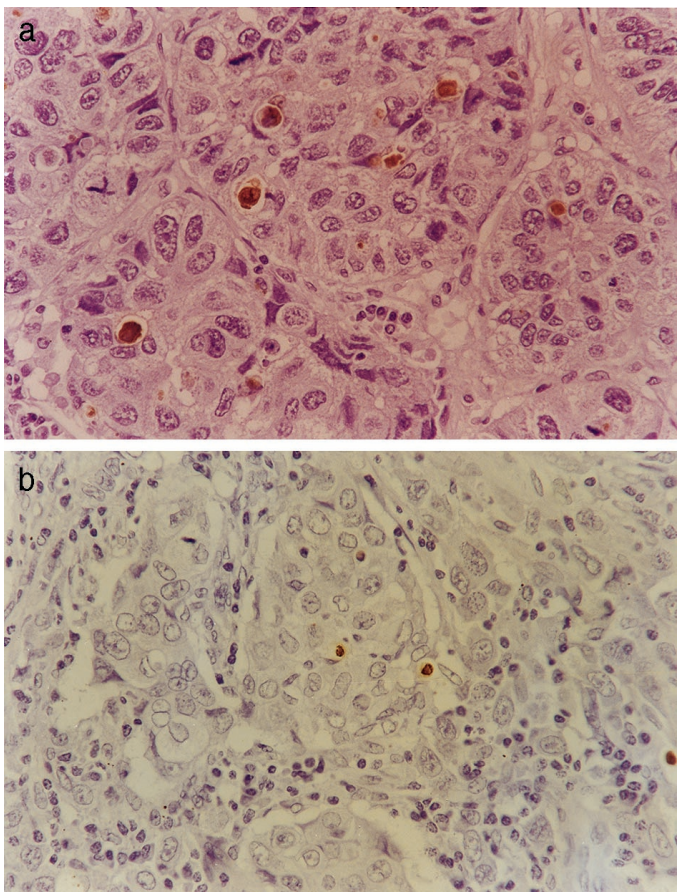

Fig. 8. *a*, squamous cell lung carcinoma (case 20) with high AI (3.5%). TUNEL (DAB as chromogen; see "Materials and Methods") and hematoxylin counterstain (×400). *b*, squamous cell lung carcinoma (case 57) with a low AI (1.8%). TUNEL (DAB as chromogen; see "Materials and Methods") and hematoxylin counterstain (×400).

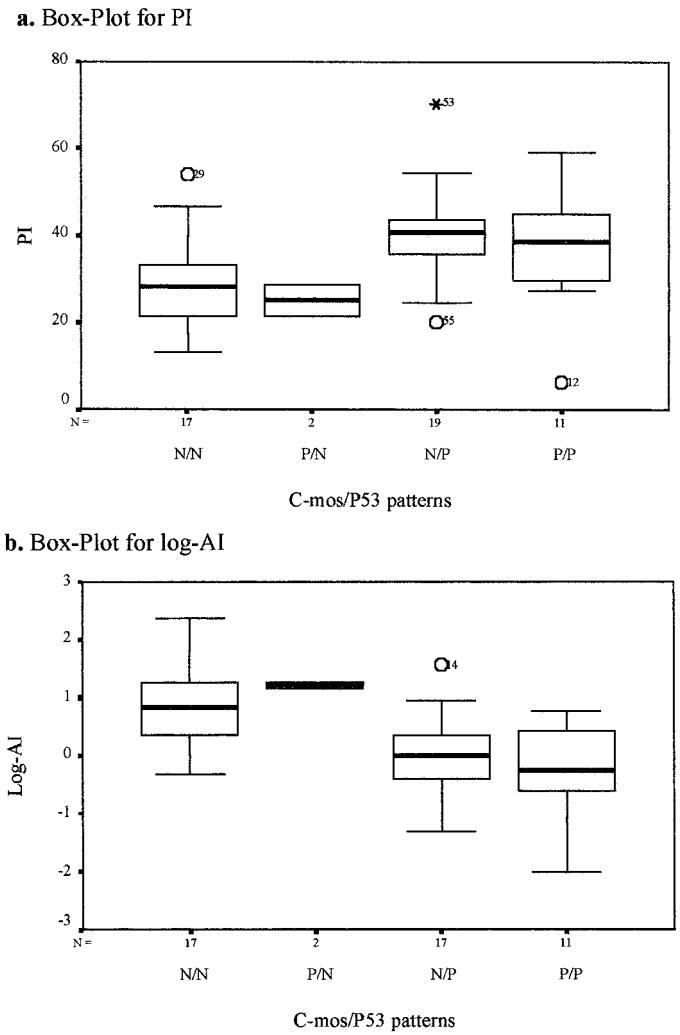

Fig. 9. Box-plots present the PI (*a*) and AI (*b*) of tumors with certain protein expression profiles.

erative activity ($P = 0.004$), decreased apoptotic rate ($P < 0.001$), and genomic instability (aneuploidy; $P = 0.005$) compared with the group of patients with normal p53 status (Table 2) underscores the central role of wt p53 as the cellular gatekeeper of growth and division (62).

These data lead to speculation as to the role of c-mos overexpression in a cancerous cell, because its relationship with tumor kinetics and genomic instability seems mainly to be dependent on the integrity of p53. One possible explanation is that overexpressed c-mos may bypass various G_0 steps, normally initiated by growth factors, that render the tumor cells insensitive to and independent of growth regulatory signals. Support for this hypothesis derives from a recent study (63) that exhibited that v-*mos* transformed murine fibroblasts were characterized by rapid growth and decreased serum requirements while simultaneously inhibiting platelet-derived growth factor-mediated signal transduction. Additional evidence comes from the reports of Rhodes *et al.* (20) and Afshari *et al.* (21), who showed that serum-starved v-*mos*-transformed NIH3T3 cells were unable to down-regulate the activity of critical cell cycle regulatory molecules, which included cyclins D, E, and A, cyclin dependent kinases, and S-phase specific E2F complexes. In an attempt to examine the downstream biochemical effects of c-mos overexpression, we studied the status of phosphorylated ERK1/2, but we did not find any differences between the c-mos(P) and c-mos(N) groups. This finding is expected because ERKs are activated by numerous upstream signals (38). In keeping with the latter, we observed that the c-mos(N) cases were accompanied with K-ras mutations, whereas the c-mos(P) cases possessed none. This observation implies alternative modes of activation of the Ras/Raf/MEK/ERK pathway.[3] Interestingly, the two c-mos(P) cases without p53 alterations were aneuploid. In this particular subset of tumors, genomic instability may be the outcome of p53 independent mechanisms (reviewed in Ref. 1) in which c-mos could be implicated (22, 39). In such a process, constitutive maintenance of maturation-promoting factor during late S phase could result in premature chromosome condensation events generating free DNA ends, which are highly recombinogenic (64). Nevertheless, the small number of c-mos(P)/p53(N) cases renders the above suggestion speculative. It is noteworthy that these cases were adenocarcinoma cells and, compared with squamous cells and small cell lung carcinomas, adenocarcinoma cells exhibit the lowest *p53* mutation rates (36). Finally, because sensitivity to certain microtubule-active drugs depends on p53 repression of microtubule-associated protein 4 (65) and c-mos activates the microtubule-associated protein kinase cascade (66, 67), the pattern of c-mos and p53 status may help in certain cases to determine the appropriate chemotherapeutic strategy.

Another interesting finding was that four c-mos(N) cases (8.5%) showed AIm at the *D8S285* locus, which lies at the telomeric boundary of c-*mos* (Table 1). This relatively low incidence is in agreement to the observed lack of c-*mos* gene amplification. Given the latter, AIm in these four cases reflects allele loss rather than amplification. This might seem inconsistent with its role as an oncogene (68) in these cases. One explanation is that LOH at *D8S285* causes loss of activity to a novel tumor suppressor gene. Yet, in case that allelic loss applies to c-*mos*, then its role in these tumors is even more complicated. Two studies (69, 70) using c-*mos*$^{-/-}$ knockout mice showed that female mutants had an elevated risk of developing ovarian teratomas, but male mutants were phenotypically normal. A plausible interpretation for our result is that because c-mos, as an MKKK, is located at the "intersection" of the MAPK pathway, its deletion, in this group of carcinomas, may play a complementary role to the actions of another defected molecule thus permitting the cancerous cell to survive. The finding of Teng *et al.* (71), who detected deletions of *MKK4* in various cell lines, is in keeping with our results.

To summarize, we have obtained evidence that c-mos protein is relatively frequently overexpressed, attributable to increased transcription, in NSCLCs. Its effects on tumor kinetics and genomic instability seem to depend mainly on the integrity of p53.

ACKNOWLEDGMENTS

We would like to thank Prof. Seth Love, Dr. Thanos D. Halazonetis, and Dr. Tariq Enver for their valuable guidance in completing our manuscript.

REFERENCES

1. Lengauer, C., Kinzler, K. W., and Vogelstein, B. Genetic instabilities in human cancers. Nature (Lond.), *396:* 643–649, 1998.
2. Arzimanoglou, I. I., Gilbert, F., and Barber, H. R. Microsatellite instability in human solid tumors. Cancer (Phila.), *82:* 1808–1820, 1998.
3. Elledge, S. J. Cell cycle checkpoints: preventing an identity crisis. Science (Washington DC), *274:* 1664–1672, 1996.
4. Prives, C., and Hall, P. A. The p53 pathway. J. Pathol., *187:* 112–126, 1999.

[3] Athanassios Kotsinas, Panayotis Zacharatos, and Vassilis Gorgoulis. Oncogenic activation of K-ras and deregulated expression of c-mos are mutually exclusive in non-small cell lung carcinomas: relationship with p53 status and tumor kinetics, submitted for publication.

5. Serrano, M., Lin, A. W., McCurrach, M. E., Beach, D., and Lowe, S. W. Oncogenic ras provokes premature cell senescence associated with accumulation of p53 and p16INK4a. Cell, *88:* 593–602, 1997.
6. Wahl, A. F., Donaldson, K. L., Fairchild, C., Lee, F. Y., Foster, S. A., Demers, G. W., and Galloway, D. A. Loss of normal p53 function confers sensitization to Taxol by increasing G2/M arrest and apoptosis. Nat. Med., *2:* 72–79, 1996.
7. Greenblatt, M. S., Bennett, W. P., Hollstein, M., and Harris, C. C. Mutations in the *p53* tumor suppressor gene: clues to cancer etiology and molecular pathogenesis. Cancer Res., *54:* 4855–4878, 1995.
8. Banin, S., Moyal, L., Shieh, S., Taya, Y., Anderson, C. W., Chessa, L., Smorodinsky, N. I., Prives, C., Reiss, Y., Shiloh, Y., and Ziv, Y. Enhanced phosphorylation of p53 by ATM in response to DNA damage. Science (Washington DC), *281:* 1674–1677, 1998.
9. Milczarek, G. J., Martinez, J., and Bowden, G. T. p53 phosphorylation: biochemical and functional consequences. Life Sci., *60:* 1–11, 1997.
10. Fuchs, S. Y., Adler, V., Pincus, M. R., and Ronai, Z. MEKK1/JNK signaling stabilizes and activates p53. Proc. Natl. Acad. Sci. USA, *95:* 10541–10546, 1998.
11. Fukasawa, K., and Vande Woude, G. F. Synergy between the Mos/mitogen-activated protein kinase pathway and loss of p53 function in transformation and chromosome instability. Mol. Cell. Biol., *17:* 506–518, 1997.
12. Watson, R., Oskarson, M., and Vande Woude, G. F. Human DNA sequence homologous to the transforming gene (*mos*) of Moloney murine sarcoma virus. Proc. Natl. Acad. Sci. USA, *79:* 4078–4083, 1982.
13. Caubert, J. F., Matthieu-Mahul, D., Bernheim, A., Larsen, C. J., and Berger, R. Human proto-oncogene c-*mos* maps to 8q11. EMBO J., *4:* 2245–2248, 1985.
14. Sagata, N. What does Mos do in oocytes and somatic cells? BioEssays, *19:* 13–21, 1997.
15. Choi, T., Fukasawa, K., Zhou, R., Tessarollo, L., Borror, K., Resau, J., and Vande Woude, G. F. The mos/mitogen-activated protein kinase (MAPK) pathway regulates the size and degradation of the first polar body in maturing mouse oocytes. Proc. Natl. Acad. Sci. USA, *93:* 7032–7035, 1996.
16. Li, C-CH., Chen, E., O'Connell, C. D., and Longo, D. L. Detection of c-*mos* proto-oncogene expression in human cells. Oncogene, *8:* 1685–1691, 1993.
17. Oskarsson, M., McClements, W. L., Blair, D. G., Maizel, J. V., and Vande Woude, G. F. Properties of a normal mouse cell DNA sequence (sarc) homologous to the src sequence of Moloney sarcoma virus. Science (Washington DC), *297:* 1222–1224, 1980.
18. Kolch, W. Meaningful relationships: the regulation of the Ras/Raf/MEK/ERK pathway by protein interactions. J. Biochem. (Tokyo), *351:* 289–305, 2000.
19. Okazaki, K., and Sagata, N. The Mos/MAP kinase pathway stabilizes c-Fos by phosphorylation and augments its transforming activity in NIH 3T3 cells. EMBO J., *14:* 5048–5059, 1995.
20. Rhodes, N., Innes, C. L., Propst, F., and Paules, R. S. Serum starved v-mos-transformed cells are unable to appropriately downregulate cyclins and CDKs. Oncogene, *14:* 3017–3027, 1997.
21. Afshari, C. A., Rhodes, N., Paules, R. S., and Mudryj, M. Deregulation of specific E2F complexes by v-mos oncogene. Oncogene, *14:* 3029–3038, 1997.
22. Fukasawa, K., and Vande Woude, G. F. Mos overexpression in Swiss 3T3 cells induces meiotic-like alterations of the mitotic spindle. Proc. Natl. Acad. Sci. USA, *92:* 3430–3434, 1995.
23. World Health Organization. The World Health Organization histologic typing of lung tumors. Am. J. Clin. Pathol., *77:* 123–136, 1982.
24. Gorgoulis, V. G., Zacharatos, P., Kotsinas, A., Liloglou, T., Kyroudi, A., Veslemes, M., Rassidakis, A., Halazonetis, T. D., Field, J. K., and Kittas, C. Alterations of the p16-pRb pathway and the chromosome locus 9p21–22 in non-small-cell lung carcinomas: relationship with p53 and MDM2 protein expression. Am. J. Pathol., *153:* 1749–1765, 1998.
25. Fukasawa, K., Zhou, R., Matten, W. T., Armstrong, A. J., Daar, I., Oskarsson, M., Sathyanarayana, B. K., Maclvor, L., Wood, T. G., and Vande Woude, G. F. Mutagenic analysis of functional domains of the mos proto-oncogene and identification of the sites important for MAPK activation and DNA binding. Oncogene, *11:* 1447–1457, 1995.
26. Athanasiou, A., Gorgoulis, V. G., Zacharatos, P., Mariatos, G., Kotsinas, A., Liloglou, T., Karameris, A., Foukas, P., Manolis, E. N., Field, J. K., and Kittas, C. c-mos immunoreactivity is an indicator of good prognosis in lung cancer. Histopathology (Oxf.), *37:* 45–54, 2000.
27. Davis, L. G., Dibner, M. D., and Battey, J. F. (eds.) Basic Methods in Molecular Biology, pp. 47–50. New York: Elsevier Science Publishing Co., Inc., 1986.
28. Gorgoulis, V. G., Zacharatos, P., Kotsinas, A., Mariatos, G., Liloglou, T., Vogiatzi, T., Foukas, P., Rassidakis, G., Garinis, G., Ioannides, T., Zoumpourlis, V., Bramis, J., Michail, P. O., Asimacopoulos, P. J., Field, J. K., and Kittas, C. Altered expression of the cell cycle regulatory molecules pRb, p53, and MDM2 exert a synergetic effect on tumor growth and chromosomal instability in non-small cell lung carcinomas (NSCLCs). Mol. Med., *6:* 208–237, 2000.
29. Van Beveren, C., Galleshaw, J. A., Jonas, V., Berns, A. J., Doolittle, R. F., Donoghue, D. J., and Verma, I. M. Nucleotide sequence and formation of the transforming gene of a mouse sarcoma virus. Nature (Lond.), *289:* 258–262, 1981.
30. Gorgoulis, V., Tsatsanis, C., Ozanne, B., and Spandidos, D. A. Detection of epidermal growth factor receptor and c-erbB-2 gene amplification in transitional cell bladder carcinoma using the differential PCR technique. Int. J. Oncol., *4:* 1191–1197, 1994.
31. Liloglou, T., Maloney, P., Xinarianos, G., Fear, S., and Field, J. K. Sensitivity and limitations of high throughout fluorescent microsatellite analysis for the detection of allelic imbalance. Application in lung tumours. Int. J. Oncol., *16:* 5–14, 2000.
32. Auer, G. U., Falkmer, U. G., and Zetterberg, A. D. Image cytometric nuclear DNA analysis in clinical tumor material. *In:* J. P. A. Baak (ed.), Manual of Quantitative Pathology in Cancer Diagnosis and Prognosis, pp. 211–232. Heidelberg: Springer, 1991.
33. Hirano, T., Franzen, B., Kato, H., Ebihara, Y., and Auer, G. Genesis of squamous cell lung carcinoma. Sequential changes of proliferation, DNA ploidy, and p53 expression. Am. J. Pathol., *144:* 296–302, 1994.
34. Gavrieli, Y., Serman, Y., and Ben Sasson, S. Identification of programmed cell death *in situ* via specific labeling of nuclear DNA fragmentation. J. Cell Biol., *119:* 493–501, 1992.
35. Kawai, T., Suzuki, M., Kono, S., Shinomiya, N., Rokutanda, M., Takagi, K., Ogata, T., and Tamai, S. Proliferating cell nuclear antigen and Ki-67 in lung carcinoma: correlation with DNA flow cytometric analysis. Cancer (Phila.), *74:* 2468–2475, 1994.
36. Sekido, Y., Fong, K. M., and Minna, J. D. Progress in understanding the molecular pathogenesis of human lung cancer. Biochim. Biophys. Acta, *1378:* 21–59, 1998.
37. Propst, F., Rosenberg, M. P., Iyer, A., Kaul, K., and Vande Woude, G. F. c-mos proto-oncogene RNA transcripts in mouse tissues: structural features, developmental regulation and localization in specific cell types. Mol. Cell. Biol., *7:* 1629–1637, 1987.
38. Lewis, T. S., Shapiro, P. S., and Ahn, N. G. Signal transduction through MAP kinase cascades. Adv. Cancer Res., *74:* 49–139, 1998.
39. Min Wang, X., Yew, N., Peloquin, J. G., Vande Woude, G. F., and Borisy, G. G. Mos oncogene product associates with kinetochores in mammalian somatic cells and disrupts mitotic progression. Proc. Natl. Acad. Sci. USA, *91:* 8329–8333, 1994.
40. Yew, N., Strobel, M., and Vande Woude, G. F. Mos and the cell cycle: the molecular basis of the transformed phenotype. Curr. Opin. Genet. Dev., *3:* 19–25, 1993.
41. Watson, P. H., Safneck, J. R., Le, K., Dubik, D., and Shiu, R. P. Relationship of c-myc amplification to progression of breast cancer from *in situ* to invasive tumor and lymph node metastasis. J. Natl. Cancer Inst. (Bethesda), *85:* 902–907, 1993.
42. Xu, W., and Cooper, G. M. Identification of a candidate c-mos repressor that restricts transcription of germ cell-specific genes. Mol. Cell. Biol., *15:* 5369–5375, 1995.
43. Parkar, M. H., Seid, J. M., Stringer, B. M., Ingemansson, S., Woodhouse, N., and Goyns, M. H. Abnormal expression of the MOS proto-oncogene in human thyroid medullary carcinoma. Cancer Lett., *43:* 185–189, 1988.
44. Danos, O., and Yavin, M. Cancer cells: oncogenes and viral genes. *In:* G. F. Vande Woude, A. J. Levine, W. C. Topp, and J. D. Watson (eds.), vol. 2, pp. 291–294. Cold Spring Harbor, NY: Cold Spring Harbor Laboratory, 1984.
45. Gorgoulis, V. G., Zacharatos, P., Kotsinas, A., Kyroudi, A., Rassidakis, A. N., Ikonomopoulos, J. A., Barbatis, C., Herrington, C. S., and Kittas, C. Human papilloma virus (HPV) is possibly involved in laryngeal but not in lung carcinogenesis. Hum. Pathol., *30:* 274–283, 1999.
46. Slebos, R. J., Evers, S. G., Wagenaar, S. S., and Rodenhuis, S. Cellular protooncogenes are infrequently amplified in untreated non-small cell lung cancer. Br. J. Cancer, *59:* 76–80, 1989.
47. Gasperi-Campani, A., Roncuzzi, L., Ricotti, L., Lenzi, L., Gruppioni, R., Sensi, A., Zini, N., Zoli, W., and Amadori, D. Molecular and biological features of two new human squamous and adenocarcinoma of the lung cell lines. Cancer Genet. Cytogenet., *107:* 11–20, 1998.
48. Leonard, J. H., Kearsley, J. H., Chenevix-Trench, G., and Hayward, N. K. Analysis of gene amplification in head-and-neck squamous-cell carcinoma. Int. J. Cancer, *48:* 511–515, 1991.
49. Ranzani, G. N., Pellegata, N. S., Previdere, C., Saragoni, A., Vio, A., Maltoni, M., and Amadori, D. Heterogeneous proto-oncogene amplification correlates with tumor progression and presence of metastases in gastric cancer patients. Cancer Res., *50:* 7811–7814, 1990.
50. Stenman, G., Sahlin, P., Mark, J., and Landys, D. Structural alterations of the c-mos locus in benign pleomorphic adenomas with chromosome abnormalities of 8q12. Oncogene, *6:* 1105–1108, 1991.
51. Eng, C., Foster, K. A., Healey, C. S., Houghton, C., Gayther, S. A., Mulligan, L. M., and Ponder, B. A. Mutation analysis of the c-mos proto-oncogene and the endothelin-B receptor gene in medullary thyroid carcinoma and pheochromocytoma. Br. J. Cancer, *74:* 339–341, 1996.
52. de Foy, K. A., Gayther, S. A., Colledge, W. H., Crockett, S., Scott, I. V., Evans, M. J., and Ponder, B. A. Mutation analysis of the c-mos proto-oncogene in human ovarian teratomas. Br. J. Cancer, *77:* 1642–1644, 1998.
53. Nishizawa, M., Okazaki, K., Furuno, N., Watanabe, N., and Sagata, N. The 'second-codon rule' and autophosphorylation govern the stability and activity of Mos during the meiotic cell cycle in *Xenopus* oocytes. EMBO J., *11:* 2433–2446, 1992.
54. Pham, C. D., Vuyyuru, V. B., Yang, Y., Bai, W., and Singh, B. Evidence for an important role of serine 16 and its phosphorylation in the stabilization of c-Mos. Oncogene, *18:* 4287–4294, 1999.
55. Chen, M., and Cooper, J. A. Ser-3 is important for regulating Mos interaction with and stimulation of mitogen-activated protein kinase kinase. Mol. Cell. Biol., *15:* 4727–4734, 1995.
56. Matten, W. T., Copeland, T. D., Ahn, N. G., and Vande Woude, G. F. Positive feedback between MAP kinase and Mos during *Xenopus* oocyte maturation. Dev. Biol., *179:* 485–492, 1996.
57. Mansour, S. J., Matten, W. T., Hermann, A. S., Candia, J. M., Rong, S., Fukasawa, K., Vande Woude, G. F., and Ahn, N. G. Transformation of mammalian cells by constitutively active MAP kinase kinase. Science (Washington DC), *265:* 966–970, 1994.
58. Benayoun, B., Pelpel, K., Solhonne, B., Guillier, M., and Leibovitch, S. A. Overexpression of Mos(rat) proto-oncogene product enhances the positive autoregulatory loop of MyoD. FEBS Lett., *437:* 39–43, 1998.
59. Fukasawa, K., Rulong, S., Resau, J., Pinto da Silva, P., and Vande Woude, G. F. Overexpression of mos oncogene product in Swiss 3T3 cells induces apoptosis preferentially during S-phase. Oncogene, *10:* 1–8, 1995.

60. Hicks, G. G., Egan, S. E., Greenberg, A. H., and Mowat, M. Mutant p53 tumor suppressor alleles release ras-induced cell cycle growth arrest. Mol. Cell. Biol., *11:* 1344–1352, 1991.
61. Damalas, A., Ben-Ze'ev, A., Simcha, I., Shtutman, M., Leal, J. F., Zhurinsky, J., Geiger, B., and Oren, M. Excess β-catenin promotes accumulation of transcriptionally active p53. EMBO J., *18:* 3054–3063, 1999.
62. Levine, A. J. p53, the cellular gatekeeper for growth and division. Cell, *88:* 323–331, 1997.
63. Faller, D. V., Mundschau, L. J., Forman, L. W., and Quinones, M. A. v-mos suppresses platelet-derived growth factor (PDGF) type-β receptor autophosphorylation and inhibits PDGF-BB-mediated signal transduction. J. Biol. Chem., *269:* 5022–5029, 1994.
64. Vande Woude, G. F. Mos. *In:* G. Hardie and S. Hanks (eds.), The Protein Kinase Factsbook, pp. 358–360. London: Academic Press, 1995.
65. Zhang, C. C., Yang, J-M., Bash-Babula, J., White, E., Murphy, M., Levine, A. J., and Hait, W. N. DNA damage increases sensitivity to *Vinca* alkaloids and decreases sensitivity to Taxanes through p53-dependent repression of microtubule-associated protein 4. Cancer Res., *59:* 3663–3670, 1999.
66. Yew, N., Melini, M. L., and Vande Woude, G. F. Meiotic initiation by the *mos* protein in *Xenopus*. Nature (Lond.), *355:* 649–652, 1992.
67. Hunt, T. Cell cycle arrest and c-mos. Nature (Lond.), *355:* 587–588, 1992.
68. Schulz, N., Propst, F., Rosenberg, M. P., Linnoila, R. I., Paules, R. S., Kavztch, R., Ogiso, Y., and Vande Woude, G. F. Pheochromocytomas and C-cell thyroid neoplasms in transgenic c-mos mice: a model for the human multiple endocrine neoplasia type 2 syndrome. Cancer Res., *52:* 450–452, 1992.
69. Colledge, W. H., Carlton, M. B., Udy, G. B., and Evans, M. J. Disruption of c-mos causes parthenogenetic development of unfertilized mouse eggs. Nature (Lond.), *370:* 65–68, 1994.
70. Hashimoto, N., Watanabe, N., Furuta, Y., Tamemoto, H., Sagata, N., Yokoyama, M., Okazaki, K., Nagayoshi, M., Takeda, N., Ikawa, Y., *et al.* Parthenogenetic activation of oocytes in c-mos-deficient mice. Nature (Lond.), *370:* 68–71, 1994.
71. Teng, D. H., Perry, W. L., III, Hogan, J. K., Baumgard, M., Bell, R., Berry, S., Davis, T., Frank, D., Frye, C., Hattier, T., *et al.* Human mitogen-activated protein kinase kinase 4 as a candidate tumor suppressor. Cancer Res., *57:* 4177–4182, 1997.

Deregulated Expression of c-*mos* in Non-Small Cell Lung Carcinomas: Relationship with *p53* Status, Genomic Instability, and Tumor Kinetics

Vassilis G. Gorgoulis, Panayotis Zacharatos, George Mariatos, et al.

Cancer Res 2001;61:538-549.